Journal of Power Sources 196 (2011) 9590–9598

Contents lists available at ScienceDirect

Journal of Power Sources

journal homepage: www.elsevier.com/locate/jpowsour

Effect of the preparation method on the performance of CuO–MnO_x–CeO_2 catalysts for selective oxidation of CO in H_2-rich streams

Jing Li[a], Pengfei Zhu[a,b], Renxian Zhou[a,*]

[a] Institute of Catalysis, Zhejiang University, Hangzhou 310028, PR China
[b] School of Chemistry and Chemical Engineering, Southwest Petroleum University, Chengdu 610500, PR China

ARTICLE INFO

Article history:
Received 23 May 2011
Received in revised form 13 July 2011
Accepted 15 July 2011
Available online 22 July 2011

Keywords:
Hydrogen purification
CO selective oxidation
Copper
Manganese
Ceria support

ABSTRACT

Selective oxidation of CO in H_2-rich streams is performed over a series of CuO–MnO_x–CeO_2 catalysts prepared by hydrothermal (CuMC-HY), co-precipitation (CuMC-CP), impregnation (CuMC-IM) and citrate sol–gel (CuMC-SG) methods. The catalysts are characterized by N_2 adsorption/desorption, XRD, SEM, HR-TEM, TPR and XPS techniques. The results show that the catalyst prepared by a hydrothermal method exhibits the best catalytic activity, especially at low temperatures. The temperature of 50% CO conversion (T_{50}) is only 74 °C and the temperature window of CO conversions up to 99.0% is about 40 °C wide, from 110 to 140 °C. Moreover, the temperature window is still maintained 20 °C wide even at lower temperatures when there are 15% CO_2 and 7.5% H_2O in the reaction gas. The superior catalytic performance of CuMC-HY is attributed to the formation of Mn–Cu–Ce–O solid solution, the unique pore structure and the existence of more Cu^+ and Mn^{4+} species as well as oxygen vacancies. The sequence of catalytic activity is as follows: CuMC-HY > CuMC-SG > CuMC-IM > CuMC-CP. The worst catalytic activity, obtained from the catalyst prepared by the co-precipitation method, is possibly related to the existence of independent CuO_x and MnO_x oxides, which weakly interact with ceria in the catalyst.

1. Introduction

Polymer electrolyte membrane fuel cells (PEMFC) have been attracting more and more attention in the applications to electric vehicles or residential power-generation for their many merits, such as low operating temperature, high power density, long work time, and rapid start-up [1,2]. Although hydrogen is the ideal fuel as the only reaction product is H_2O [3], the distribution and storage of pure hydrogen has limited its use. Therefore, H_2-rich streams made from the reforming of hydrocarbons gradually become the primary fuel source of PEMFC. Nevertheless, such H_2-rich streams often contain 0.3–1% of CO, which would poison the Pt anode catalyst in the H_2-PEMFC anode [4]. Thus, CO must be removed to avoid poisoning the anode of fuel cells [5,6]. Among the present available methods, selective oxidation (PROX) of CO in H_2-rich streams is regarded as one of the promising and cost-effective methods to achieve tolerable CO concentrations (below 100 ppm) [3,7,8]. Catalysts for such a reaction request a compromise between catalytic performance and catalyst cost. Precious metal catalysts such as Au, Pt, Rh, and Ru often possess excellent catalytic performance in this reaction [9–11]. However, the high cost of precious metals has prompted researchers to look for alternative catalysts.

In the last decades, as a promising substitute for precious metal catalysts in the CO-PROX reaction in H_2-rich streams, the CuO–CeO_2 mixed oxide catalysts have received considerable attention [12–14]. They are more active and selective than Pt-based catalysts at lower reaction temperatures [15]. Nevertheless, the CuO–CeO_2 catalysts have a serious disadvantage that CO conversion is greater than 99% only in a very narrow operating temperature "window" (just 5–20 °C) [16–18]. In such a case, broadening the temperature window of complete CO conversion becomes a crucial issue for CO-PROX reaction over CuO–CeO_2 catalysts. Doping transition metals into CuO–CeO_2 catalysts is considered as an effective way to solve this issue. For example, Sirichaiprasert et al. [19] reported that α-Fe_2O_3 promoted the catalytic activities of the active species in Cu–Ce–Fe–O catalysts, due to the increase of surface area and pore volume as well as the intense interaction between CuO and CeO_2. Wu et al. [20] suggested that the doping of TiO_2 in ceria not only enhanced the surface area and decreased the particle size of the support but also promoted the dispersion of active copper species; moreover, owing to the doping of TiO_2 a stronger interaction between CuO and the support was formed, which was a major reason for the high catalytic activity of CuO/$Ce_{0.8}Ti_{0.2}O_2$. In addition, Firsova et al. [21] found that the additives of Fe and Ni oxides increased the activity of CuO–CeO_2 catalysts with a low concentration of CuO, because the introduction of both additives facilitated the formation of an additional amount of active centers related to CuO. Besides, our previous study [22] also revealed that doping an

* Corresponding author. Tel.: +86 571 88273290; fax: +86 571 88273283.
E-mail address: zhourenxian@zju.edu.cn (R. Zhou).

0378-7753/$ – see front matter © 2011 Elsevier B.V. All rights reserved.
doi:10.1016/j.jpowsour.2011.07.052

appropriate amount of Mn into CuO–CeO_2 catalysts would improve the catalytic performance for CO-PROX reaction in H_2-rich streams, owing to the formation of a more stable Cu–Mn–Ce–O solid solution and the enhancement of the redox properties of catalysts. What is more, it is well known that most of the properties, such as the formation and display of synergistic function, solid solution, Cu^+ species and oxygen vacancies, which make CuO–CeO_2 and related mixed oxides active, strongly depend on the preparation methods. For example, Kim and Cha [23] reported that the co-precipitation process facilitated the formation of synergetic interaction between copper species and CeO_2, which reduced the redox potentials of the copper species and facilitated Cu^{2+}/Cu^+ redox couple in CeO_2. Zhu et al. [24] indicated that a large number of Cu^+ were formed in the hydrothermal process, which was regarded as the active centers of CO adsorption over CuO–CeO_2 catalysts. Luo et al. [25] found that the citrate sol–gel method offered nanostructured Ce–Cu–O solid solution with higher surface area and smaller crystallite size, which resulted in higher catalytic activity for CO oxidation at low temperatures.

In this work, four CuO–MnO_x–CeO_2 catalysts were prepared using hydrothermal, co-precipitation, impregnation, and citrate sol–gel methods, respectively. All the samples were characterized by N_2 adsorption/desorption, XRD, SEM, HR-TEM, TPR and XPS techniques. The characterization results are correlated with the exhibited catalytic behavior of CuO–MnO_x–CeO_2 catalysts for CO-PROX reaction in H_2-rich streams.

2. Experimental

2.1. Preparation of catalysts

Four catalysts prepared by hydrothermal, co-precipitation, impregnation, and citrate sol–gel methods are labeled as CuMC-HY, CuMC-CP, CuMC-IM and CuMC-SG, respectively.

CuMC-HY was synthesized by a hydrothermal method. $NH_3{\cdot}H_2O$ was added to the mixed ethanol solution of $Ce(NO_3)_3{\cdot}6H_2O$, $Cu(NO_3)_2{\cdot}3H_2O$, $Mn(NO_3)_2$ and cetyltrimethyl ammonium bromide (CTAB; the molar ratio of CTAB to Ce was 1:1) with constant stirring. The pH value of the mixture solution was adjusted to 9.0, and then the mixture was aged at 100 °C for 1 h in a stainless steel autoclave. The precipitate was separated by filtration, dried at 110 °C and then calcined at 500 °C for 2 h in air.

CuMC-CP was synthesized by a co-precipitation method. Appropriate amounts of $Ce(NO_3)_3{\cdot}6H_2O$, $Cu(NO_3)_2{\cdot}3H_2O$, $Mn(NO_3)_2$ were dissolved in 100 ml distilled water, and Na_2CO_3 solution was added dropwise with continuous stirring until the pH was 9.0. The precipitate was aged with stirring at ambient temperature for 2 h. After filtration the precipitate was washed first with deionized water until the pH was 7.0, then with ethanol for three times. Subsequently, the precipitate was dried at 110 °C and then calcined at 500 °C for 2 h in air.

CuMC-SG was synthesized by a citrate sol–gel method. A mixture of $Ce(NO_3)_3{\cdot}6H_2O$, $Cu(NO_3)_2{\cdot}3H_2O$, $Mn(NO_3)_2$ was dissolved into deionized water. Then citric acid was added with two times molar amounts to the premixed solution while stirring. After that, the solution was heated in water bath until a viscous gel was obtained. The gel was dried at 110 °C, heated in the nitrogen atmosphere at 800 °C for 2 h and then calcined in air at 500 °C for 2 h.

CuMC-IM was synthesized by an impregnation method. CeO_2 support was prepared by the hydrothermal method as mentioned above. Then CeO_2 support was added to the mixed ethanol solution of $Cu(NO_3)_2{\cdot}3H_2O$ and $Mn(NO_3)_2$ with constant stirring for 12 h. The mixture was aged for 12 h, dried at 110 °C and then calcined at 500 °C for 2 h in air.

The molar ratio of Mn to Cu is 1:5 for all the catalysts with 5.0 wt% Cu and the samples were crushed and sieved to 60–80 mesh before catalytic evaluation.

2.2. Catalytic performance tests

The catalytic performance tests for CO-PROX reaction in H_2-rich streams were carried out in a fixed-bed micro-reactor (quartz glass, i.d. = 6 mm) at atmospheric pressure. 100 mg of catalyst was used in the test, which was diluted with inert α-alumina particles of the same mesh (60–80) with a mass ratio of 2:1. Prior to reactions, the samples were pretreated in oxygen at 150 °C for 0.5 h. The composition of simulative reformate gas was 1.0% CO (by volume, hereinafter), 1.0% O_2, 50% H_2, 15% CO_2 (when used), 7.5% H_2O (when used) and Ar in balance. The total flow rate was 100 ml min^{-1}, and the space velocity was 60,000 ml g^{-1} h^{-1}.

The effluent gases were measured by an on-line gas chromatograph equipped with a thermal conductivity detector (TCD) and a flame ionization detector (FID). H_2 and O_2 were separated by a carbon molecular sieve (TDX-01) column and detected by TCD. CO and CO_2 were separated by a carbon molecular sieve (TDX-01) column, and converted to methane by a methanation reactor and analyzed by FID. The detection limit of FID for CO is 3 ppm.

Taking CO_2 in the feedstock into consideration, the conversion can be calculated as follows:

$$\text{CO conversion}\,(\%) = \frac{[\text{CO}]_{\text{in}} - [\text{CO}]_{\text{out}}}{[\text{CO}]_{\text{in}}} \times 100$$

$$\text{O}_2\ \text{conversion}\,(\%) = \frac{[\text{O}_2]_{\text{in}} - [\text{O}_2]_{\text{out}}}{[\text{O}_2]_{\text{in}}} \times 100$$

The selectivity was evaluated from the oxygen mass balance as follows:

$$\text{Selectivity}\,(\%) = \frac{0.5([\text{CO}]_{\text{in}} - [\text{CO}_2]_{\text{out}})}{[\text{O}_2]_{\text{in}} - [\text{O}_2]_{\text{out}}} \times 100$$

"In" and "out" as footnotes mean inlet and outlet gaseous stream, respectively.

2.3. Characterization of catalysts

Nitrogen adsorption and desorption isotherms were determined on a Tristar II 3020 apparatus at −195.8 °C. The specific surface areas were calculated by the BET method.

The scanning electron microscope (SEM) was performed on a SIRION Analytical Scanning Electron Microscopy (FEI Corp., Holland) in order to obtain the morphological appearance of the catalysts.

High resolution transmission electron microscopy (HR-TEM) images were obtained using a JEM-2010 apparatus operated at 200 kV. The sample was prepared by dipping a copper-grid-supported transparent carbon foil in an ethanol solution, and the grid was dried in open air.

Powder X-ray diffraction (XRD) patterns were recorded on a Rigaku D/Max 2550 PC powder diffractometer using nickel-filtered Cu Kα radiation in the range of $20^\circ \le 2\theta \le 80^\circ$. The X-ray tube was operated at 40 kV and 300 mA. The average crystallite size was estimated from the line broadening with the Scherrer formula.

H_2 temperature-programmed reduction (H_2-TPR) was carried out in a quartz fixed-bed micro-reactor. In each run, 50 mg of catalyst was pretreated at 200 °C in the flow of N_2 (30 ml min^{-1}), then the sample was heated to 500 °C with a ramp of 10 °C min^{-1} in the steam of 5 vol% H_2/Ar (40 ml min^{-1}). The consumption of H_2 during the reduction was measured by TCD.

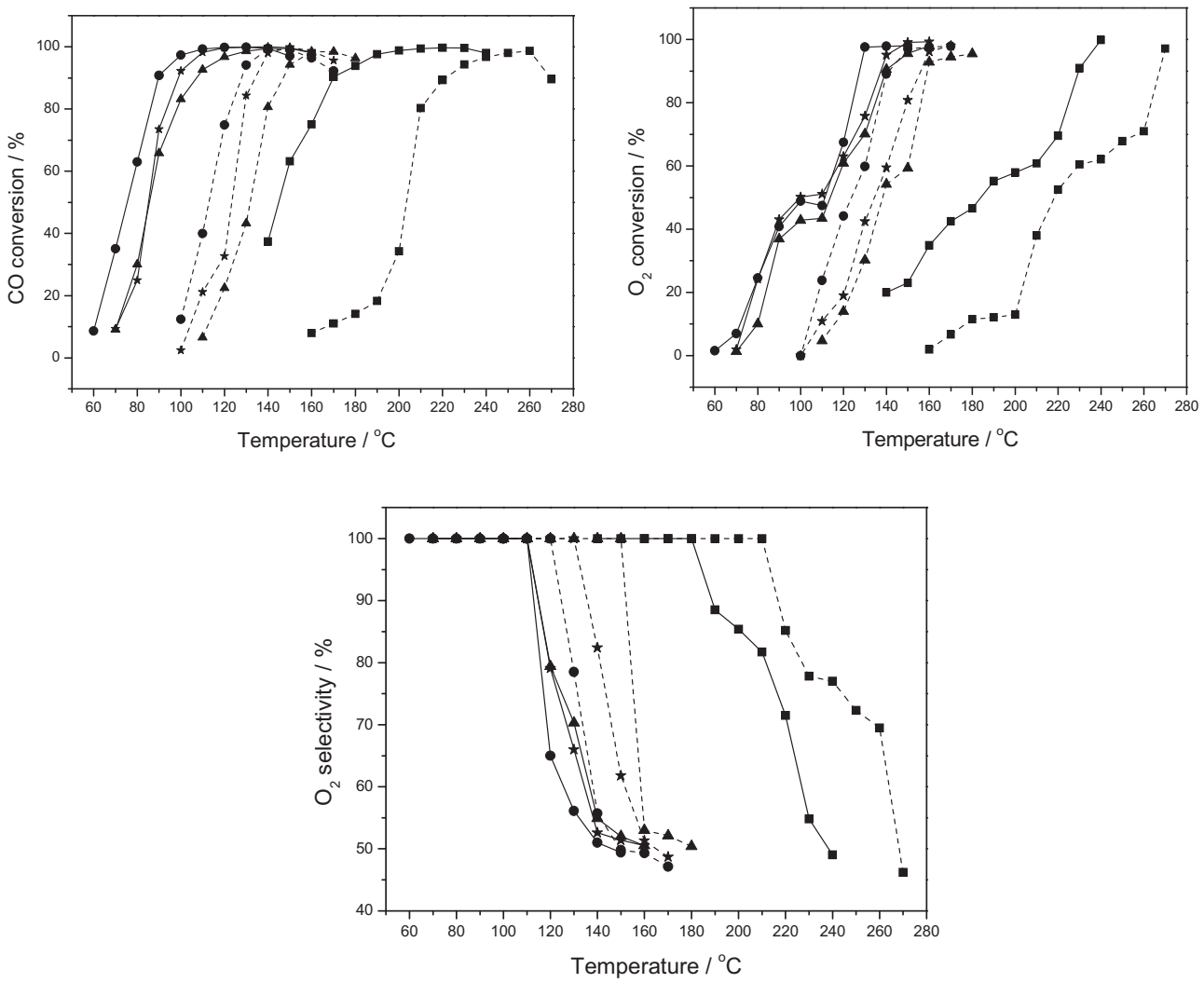

Fig. 1. The catalytic behavior of (●) CuMC-HY, (□) CuMC-SG, (▲) CuMC-IM and (■) CuMC-CP catalysts tested under (—) standard stream composed by 1% CO + 50% H_2 + 1% O_2 or (·····) mixtures additionally containing 15% CO_2 + 7.5% H_2O.

X-ray photoelectron spectroscopy (XPS) measurements were recorded with a PHI5000c spectrometer at 1486.6 eV and 12.5 kV using Al Kα radiation.

3. Results and discussion

3.1. Catalytic performance

3.1.1. Catalytic behavior of $CuO–MnO_x–CeO_2$ catalysts for CO-PROX reaction in H_2-rich streams

Fig. 1 shows the activity and selectivity of $CuO–MnO_x–CeO_2$ catalysts prepared by four different methods for CO-PROX reaction in H_2-rich streams. When no extra CO_2 and H_2O are added in the reaction gas (depicted as solid line), CuMC-HY shows the best activity, especially at low temperatures, T_{50} (the temperature of 50% of CO conversion) is only 74 °C. Moreover, CuMC-HY has a wider temperature window of about 40 °C (the temperature range of CO conversions up to 99.0%), from 110 to 140 °C. It is closely followed by CuMC-SG with a window of the same width, from 120 to 150 °C. CuMC-IM has a worse activity only with a 20 °C wide window, from 140 to 150 °C. CuMC-CP exhibits the worst activity, although it displays the best selectivity of O_2–CO oxidation reaction. The selectivity of O_2–CO oxidation reaction for the CuMC-CP catalyst is 100% at reaction temperature below 180 °C, while that for CuMC-HY and CuMC-SG is only below 110 °C and CuMC-IM is below 120 °C.

However, while the O_2 conversion maintains a sustained increase to nearly 100%, the selectivity of O_2-CO oxidation reaction for all the samples rapidly drop to about 50% after the point where CO conversion reaches about 100%. This result may be mainly due to two factors. One is that the oxidation of H_2 competing with that of CO to CO_2 occurs as a side reaction with the product of water. As reported in literature [18], a blocking effect was induced by the presence of relatively large amounts of adsorbed molecular water, which limited access of the reactant molecules to the sample surface for activated generation of the active sites for the process and the further reaction. The other is the occurrence of reverse water-gas shift reaction between carbon dioxide and hydrogen (verified by the TCD results, not listed here), which could generate a small amount of water and CO to inhibit CO to react with oxygen. Meanwhile, with the increasing of O_2 conversion, an inflection point appears on each sample curve at the beginning of H_2 oxidation due to the different reaction rate between CO and H_2 with O_2 in H_2-rich streams.

The above-mentioned reactions are performed upon the standard reactant mixtures in the absence of gases like CO_2 or H_2O. However, the H_2-rich streams obtained from reforming process

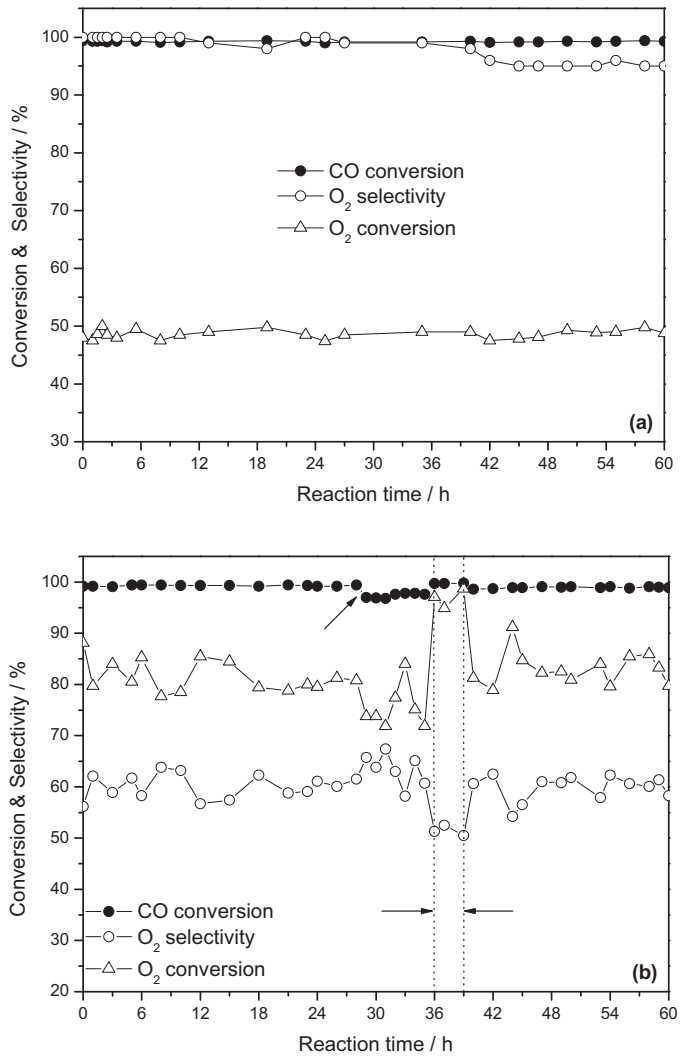

Fig. 2. Catalytic stability tests for CO-PROX reaction over the CuMC-HY catalyst in H_2-rich streams (a) without CO_2 or H_2O at 110 °C, and (b) with 15% CO_2 and 7.5% H_2O at 140 °C.

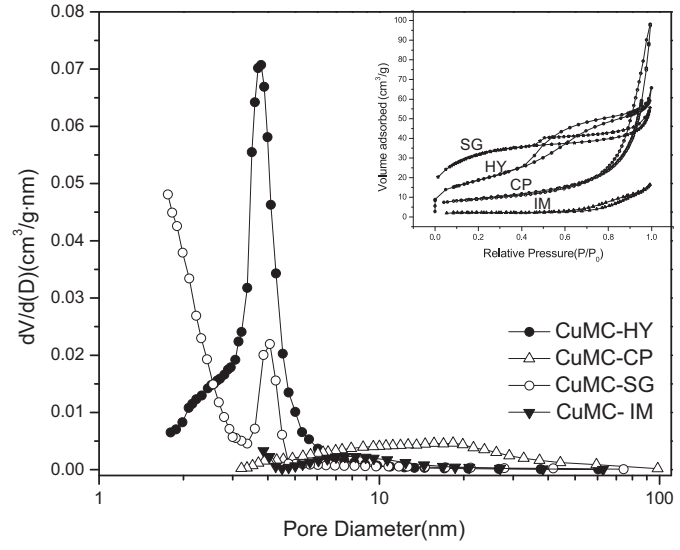

Fig. 3. BJH pore size distribution curves and N_2 adsorption–desorption isotherms (the illustration) of CuO–MnO_x–CeO_2 catalysts prepared by different methods.

also contain 15 ~ 25% CO_2 and 0 ~ 10% H_2O as well as CO and H_2. In this case, it is significant to investigate the performance of CuO–MnO_x–CeO_2 catalysts under the CO-PROX reactant mixtures in the presence of CO_2 and H_2O. Fig. 1 (depicted as dotted line) shows the influence of 15% CO_2 and 7.5% H_2O on the catalytic behavior of CuO–MnO_x–CeO_2 catalysts. Obviously, the presence of CO_2 and H_2O causes a drastic decrease in the CO oxidative activity and narrows the temperature window for CO purification to below 100 ppm (i.e. CO conversion is greater than 99.0%). Compared with the results obtained in the standard reactant mixtures without CO_2 or H_2O, the temperature windows of CuMC-HY and CuMC-SG shift from 110 ~ 140 °C and 120 ~ 150 °C to 140 ~ 150 °C and 150 °C, respectively, while those of CuMC-CP and CuMC-IM do not appear. Meanwhile, O_2 conversion also shows a sharp decline for each sample while the selectivity of O_2–CO oxidation reaction is increased, which indicates that the presence of CO_2 and H_2O inhibits the H_2 oxidation with oxygen to a certain extent. The negative effect induced by the presence of CO_2 on the catalytic behavior is related to the competitive adsorption of CO and CO_2 on the ceria surface as specific carbonates, which limits the capability for redox promotion via ceria of the generation of partially reduced CuO_x interfacial sites that are most active for CO oxidation [18,26]. The deactivating effect of H_2O in the reactant mixtures is mainly due to the blockage of the copper active sites by the adsorption of relatively large amounts of molecular water [18].

3.1.2. Stability behavior of catalyst

Fig. 2 shows the catalytic stability of CuMC-HY for CO-PROX reaction in different streams. When there is no extra CO_2 and H_2O in the reaction gas (see Fig. 2a), 99.4% CO conversion and nearly 100% O_2–CO selectivity as well as less than 50% O_2 conversion for 60 h at 110 °C are also maintained on this catalyst. However, owing to the deactivation caused by the presence of CO_2 and H_2O in the reaction gas the reaction temperature has to be raised to 140 °C in order to achieve the same CO conversion (see Fig. 2b). Moreover, the raising of reaction temperature causes O_2 conversion to increase to about 85% and O_2–CO selectivity to decrease to only about 60% on account of H_2 oxidation. In addition, it is worth noticing that the decline of CO conversion occurs after 29 h due to the presence of CO_2 and H_2O. However, the CO conversion immediately increases to 99.4% after stopping the addition of CO_2 and H_2O in the reaction gas (shown in the dashed box). Four hours later, when CO_2 and H_2O are introduced again, the CO conversion maintains about 99.1% for more than 20 hours, indicating that the negative effect of H_2O on the stability of CuMC-HY catalyst is much stronger than that of CO_2 in view of the blocking effect of adsorbed molecular water and the accumulation of carbonate species. This is in accord with the results of literatures [16,18,27].

3.2. Catalyst characterization

3.2.1. N_2 adsorption measurements

Table 1 gives the values of specific surface area calculated according to the BET method, and Fig. 3 presents the N_2 adsorption/desorption isotherms as well as the corresponding BJH pore size distribution curves of CuO–MnO_x–CeO_2 catalysts prepared by different methods. For all the samples, the BET specific surface area decreases in the sequence of CuMC-SG > CuMC-HY > CuMC-CP > CuMC-IM, differing from the sequence of catalytic activity. This observation indicates that BET specific surface area of CuO–MnO_x–CeO_2 catalysts is not the primary factor influencing catalytic activity for CO-PROX reaction in H_2-rich streams. As shown in Fig. 3, the N_2 adsorption–desorption isotherms for CuMC-HY is corresponding to type IV with an H1-type hysteresis loop, arising from the formation of large interparticle mesopores consisting of agglomerates or compacts of

Table 1
Characteristics of CuO–MnO_x–CeO_2 catalysts prepared by different methods.

Catalysts	Lattice parameter (nm)	Crystallite size (nm) d (1 1 1)	S_{BET} ($m^2\ g^{-1}$)	T_{50} (°C)
CuMC-HY	0.54107	8.7	68	74
CuMC-CP	0.54169	9.5	33	145
CuMC-SG	0.54107	5.1	109	86
CuMC-IM	0.54115	19.4	9	87

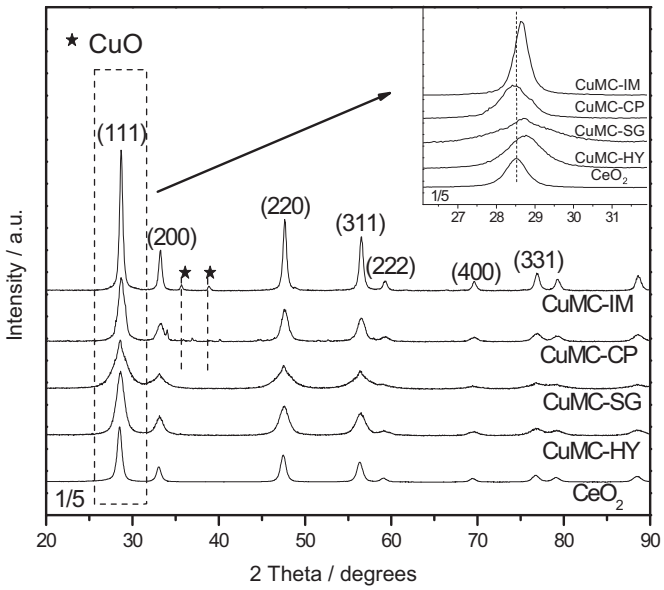

Fig. 4. XRD patterns of CuO–MnO_x–CeO_2 catalysts prepared by different methods.

approximately uniform spheres in fairly regular array [28], which indicates CuMC-HY has narrow distribution of pore size. Type IV isotherms with type H4 hysteresis loop is recorded for CuMC-SG, which is related to a mono-multilayer adsorption on the micropore and mesopore mixed adsorbent and slit-shaped pores among plate-like particles [28]. However, for CuMC-CP and CuMC-IM, the N_2 adsorption–desorption isotherms is attributed to type IV with an H3-type hysteresis loop, which does not exhibit any limiting adsorption at high P/P_0. It is observed with aggregates of plate-like particles giving rise to slit-shaped pores [28]. Moreover, the existence of types H3 and H4 implies the irregular pore structure of CuMC-SG, CuMC-CP and CuMC-IM. In addition, the distribution of mesopores for CuMC-HY, CuMC-SG, CuMC-CP and CuMC-IM are 2.7–4.6 nm, 3.3–4.5 nm, 3–44 nm and 4–25 nm, respectively. Moreover, CuMC-HY shows the narrowest mesopores distribution, suggesting that the hydrothermal process favors the formation of more orderly and narrower distribution of mesopores. Generally speaking, catalysts with orderly pores, smaller and well dispersed particles are favorable for the improvement of catalytic performance [29]. Besides, the distribution of micropores with a diameter less than 1.7 nm are observed in CuMC-SG, indicating the porous structure of CuMC-SG. The abundant micropores lead to the biggest BET specific surface area of CuMC-SG among all the samples.

3.2.2. Powder X-ray diffraction (XRD)

Fig. 4 shows the XRD patterns of CuO–MnO_x–CeO_2 catalysts prepared with different methods and Table 1 lists the lattice parameter and corresponding crystallite size, which are calculated from the (1 1 1) plane (2θ = ca. 28.7°) using Scherrer's equation. All the samples present the characteristic peaks of fluorite-type oxide structure of CeO_2 (PDF-ICDD 34-0394). No diffraction peaks corresponding to manganese oxides are found, suggesting that the manganese oxides are highly dispersed or poorly crystallized [30] or combined with the finely dispersed copper oxide and ceria to form solid solution [31].

For CuMC-HY and CuMC-SG, no crystalline peaks of copper species can be observed, which suggests that copper species are highly dispersed on the ceria surface and/or incorporated into ceria lattice to form ceria-based solid solution. Moreover, the diffraction peaks of CuMC-SG have lower intensity and are much broader than those of CuMC-HY, indicating the presence of smaller crystallites, higher specific surface area (up to 109 $m^2\ g^{-1}$) as well as poor crystallinity in CuMC-SG. According to the results of Table 1, the sequence of crystallite size is as follows: CuMC-SG < CuMC-HY < CuMC-CP < CuMC-IM. The small crystallites and high specific surface area are favorable to increasing the adsorption capacity of catalyst, which leads CuMC-SG to show excellent catalytic activity for CO oxidation. In the case of CuMC-IM, diffraction peaks corresponding to CeO_2 have the smallest values of FWHM, indicating the presence of very big crystallites, which is also in accordance with the low specific surface area. What is more, some diffraction peaks of crystalline CuO at 35.6° and 38.7° (PDF-ICDD 45-0937) are observed, arising from the aggregation of copper species on the surface of ceria, indicating that the impregnation process is not propitious for the dispersion of copper species. Big crystallites, low specific surface area and the aggregation of copper species on the surface of ceria may be disadvantageous to CO-PROX reaction in H_2-rich streams [24,27]. Fig. 4 also shows some diffraction peaks of crystalline CuO are found in the diffraction patterns of CuMC-CP. This may be related to that, in the process of co-precipitation, homogeneous co-precipitation at an atomic level is very difficult and most of the resulting precipitate is considered as a mixture of fine particles, owing to the difficulty to form co-precipitates in an alkali solution as precipitator for the considerable difference in the pH value [32] (the pH value at the beginning of the formed precipitation of Cu^{2+} is 4.7 while that of Ce^{3+} is 7.6).

Additionally, Fig. 4 shows that the diffraction peaks of CuMC-HY, CuMC-SG and CuMC-IM shift to higher 2θ value compared with that of pure CeO_2. These phenomena imply that some active components enter into ceria lattice to form solid solution, which can be confirmed from the variation of the corresponding lattice parameter of cubic CeO_2 (1 1 1), as listed in Table 1. As shown in Table 1, the lattice parameter of cubic CeO_2 (1 1 1) in the catalysts CuMC-HY and CuMC-SG are much smaller than that in the pure CeO_2 (0.54127 nm), indicating that some copper ions and manganese ions, with smaller ionic radii (the radii of Cu^{2+}, Mn^{4+}, Mn^{3+} and Mn^{2+} are 0.073, 0.056, 0.062 and 0.067 nm, respectively) than that of Ce^{4+} (0.097 nm) [22,33], enter into the ceria lattice to form Mn–Cu–Ce–O solid solution. Moreover, the more the above-mentioned ions introduced into ceria lattice are, the smaller the lattice parameter is and the more stable the formed solid solution is [34]. The existence of stable Mn–Cu–Ce–O solid solution is favorable for CO-PROX reaction in H_2-rich streams, which is the main reason for the excellent catalytic performance of CuMC-HY and CuMC-SG. The lattice parameter of cubic CeO_2 (1 1 1) in the catalyst CuMC-IM is also smaller than that of pure CeO_2, signifying a small amount of Mn–Cu–Ce–O solid solution formed in CuMC-IM, too. However, in contrast with the other three catalysts, the lattice parameter of cubic CeO_2 (1 1 1) in the catalyst CuMC-CP is much bigger than that in the pure CeO_2. It may be suggested that the

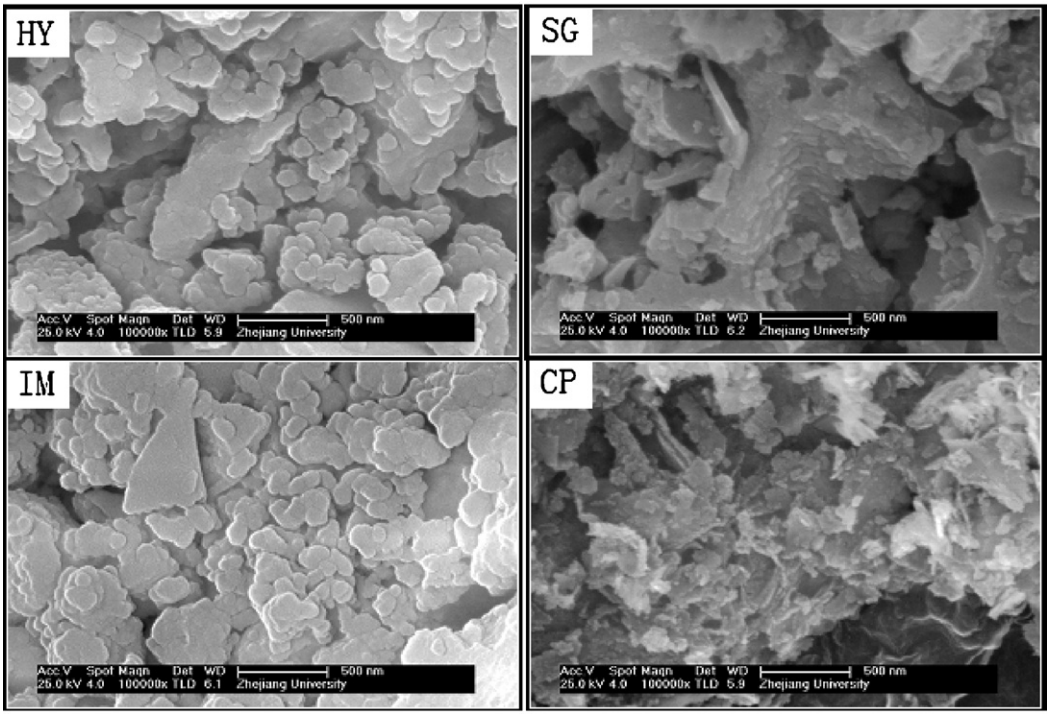

Fig. 5. SEM micrographs of CuO–MnO_x–CeO_2 catalysts prepared by different methods (scale bar = 500 nm).

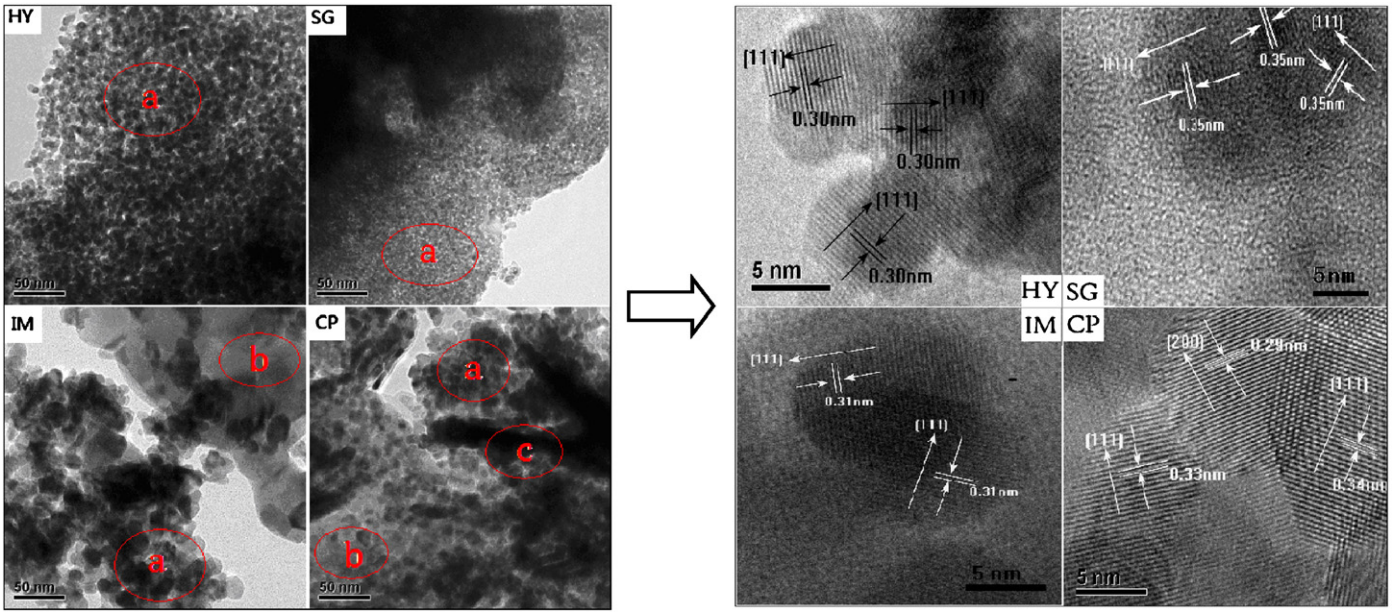

Fig. 6. TEM or HR-TEM images of CuO–MnO_x–CeO_2 catalysts prepared by different methods; (a) Mn–Cu–Ce–O solid solution as well as finely dispersed copper and manganese species on ceria, (b) CuO particles, and (c) CeO_2 particles inferred according to the results of EDX analysis.

independent CuO_x and MnO_x oxides exist on the surface of ceria and substoichiometric fluorite-structured CeO_{2-x} may be formed for the bigger ionic radius of Ce^{3+} (0.103 nm) than that of Ce^{4+} [32].

3.2.3. Scanning electron microscope (SEM)

Fig. 5 gives the SEM micrographs of CuO–MnO_x–CeO_2 catalysts prepared by different methods. The results show that the preparation methods markedly influence the catalyst morphologies. CuMC-HY and CuMC-IM present homogeneous and mostly circular-sheet particles, whereas CuMC-SG and CuMC-CP show elongated particles with irregular sizes and shape. In addition, compared with CuMC-HY, CuMC-IM exhibits some larger particles and the bulk grains due to the aggregation of small particles.

3.2.4. High-resolution transmission electron microscopy (HR-TEM)

Fig. 6 (left) displays TEM images of the four samples. As shown in Fig. 6 (left), the particles of CuMC-HY and CuMC-SG are well dispersed and much smaller than those of the other two samples. According to the results of EDX (Energy-dispersive X-ray spectroscopy, not listed here) analysis, the main form of components in CuMC-HY and CuMC-SG may be Mn–Cu–Ce–O solid solution as

Table 2
Surface contents of Cu and Mn as well as composition of Cu and Mn species derived by XPS.

Sample	Cu/(Cu + Ce + Mn) (at.%)	Mn/(Cu + Ce + Mn) (at.%)	Cu (%)[a]		Mn (%)			$Ce^{3+}3d_{5/2}$ in Ce (%)
			Cu^{+}	Cu^{2+}	Mn^{2+}	Mn^{3+}	Mn^{4+}	
CuMC-HY	19.0	7.0	29.1	70.9	21.4	34.6	46.0	17.0
CuMC-SG	25.4	4.6	4.1	95.9	35.7	33.2	31.1	14.8
CuMC-CP	28.7	2.3	4.7	95.3	47.7	33.8	18.5	18.1
CuMC-IM	37.7	8.8	17.6	82.4	30.7	33.5	35.8	14.0

[a] Calculated from the deconvolution of peaks for the kinetic energy spectra of the Auger L_3VV electron of samples.

well as the finely dispersed copper and manganese species on the ceria surface, the existence of which is one main reason for the high activity of CO PROX. This result is in good agreement with the analyzed results of XRD. However, the existence of independent oxides of CuO_x, MnO_x and CeO_x in CuMC-CP and the appearance of serious aggregation of copper species on the surface of CeO_2 in CuMC-IM may decrease their catalytic activity for CO-PROX reaction in H_2-rich streams, although both of them may contain a small amount of Mn–Cu–Ce–O solid solution as well as some finely dispersed copper and manganese species.

In order to further observe the influence of preparation methods on catalyst structure, studies by HR-TEM technique were performed and the results are shown in Fig. 6 (right). The results show that the CeO_2 (1 1 1) crystal plane space of CuMC-HY (0.30 nm), the smallest among the four samples, is smaller than that of the pure CeO_2 (0.31 nm), suggesting that some copper and manganese ions incorporate into the ceria lattice. This is because the incorporation of copper and manganese ions with smaller ionic radii into ceria lattice can induce the shrinkage of ceria crystal plane space. In addition, CuMC-IM shows similar CeO_2 (1 1 1) crystal plane space to that of the pure CeO_2, indicating small amount of copper and manganese ions incorporates into the ceria lattice. However, the CeO_2 (1 1 1) crystal plane space of CuMC-SG, about 0.35 nm, is much bigger than that of the pure CeO_2 while the main form of components is the Mn–Cu–Ce–O solid solution, based on the results of XRD analysis. This may be related to the crystal size variation. As detailed in literatures [35,36], the decrease of the crystal size can be able to increase the lattice plane space while the incorporation of copper and manganese ions into the ceria lattice decreases the lattice plane space. According to the results of XRD, the crystallite size of CuMC-SG is much smaller than that of CuMC-HY, whereas the lattice parameter of cubic CeO_2 (1 1 1) in the catalyst CuMC-SG is similar to that in the catalyst CuMC-HY, indicating that the increase of lattice plane space of CuMC-SG is mainly caused by the presence of small crystallites resulted from the poor crystallinity. Besides, CuMC-CP also shows a bigger value of the CeO_2 (1 1 1) crystal plane space than that of the pure CeO_2, which may be the result of the presence of some Ce^{3+} species in the ceria lattice for the bigger ionic radius of Ce^{3+} than that of Ce^{4+}. Moreover, some CeO_2 (2 0 0) crystal planes are observed in the HR-TEM images of CuMC-CP. The (2 0 0) plane has worse stability than the (1 1 1) plane, due to that the (1 1 1) plane is most thermodynamically stable on the surface of CeO_2 and considered to be the preferentially exposed plane of $CuO–CeO_2$ catalysts with fluorite structures [37].

3.2.5. Temperature-programmed reduction with H_2 (H_2-TPR)

Fig. 7 presents the H_2-TPR profiles of $CuO–MnO_x–CeO_2$ catalysts prepared by different methods. Under our experimental conditions, the reduction peaks of cerium oxide are not observed below ca. 400 °C. Additionally, manganese oxides present a lower reducibility than copper oxides due to the more negative free energy of formation of manganese oxides in comparison to that of copper oxides. Furthermore, coexistence of copper ions and manganese ions can be mutually facilitating each other's reduction, so their reduction peaks are difficult to distinguish [38–40].

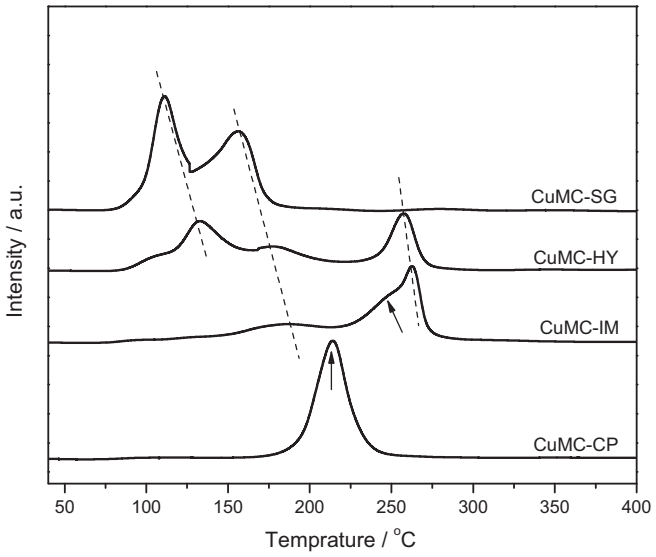

Fig. 7. H_2-TPR profiles of $CuO–MnO_x–CeO_2$ catalysts prepared by different methods.

As shown in Fig. 7, there are two reduction peaks in the H_2 consumption profiles of CuMC-HY and CuMC-SG below ca. 220 °C. The low-temperature reduction peak is attributed to some manganese and copper species which strongly interact with ceria, while the high-temperature reduction peak is attributed to the reduction of dispersed CuO_x species on the surface of CeO_2, including isolated Cu^{2+} ions that weakly interact with CeO_2 and the two- and three-dimensional copper clusters in small size [41]. The temperatures of the former two peaks for CuMC-SG are lower than those for CuMC-HY, respectively, owing to the smaller size of particles in the sample prepared with the citrate sol–gel method than those with the hydrothermal method. Besides, there is a peak, ascribed to the reduction of stable Cu^{+} species at about 257 °C [24], shown in the H_2 consumption profile of CuMC-HY, which may be a result of strong interaction between active components and support. Many studies [42,43] show that Cu^{+} species are the main adsorptive and active centers of CO. So we can infer that the presence of stable Cu^{+} species in CuMC-HY may be one of the main reasons for its higher catalytic activity of CO oxidation than CuMC-SG.

For CuMC-CP, there is only one reduction peak at about 214 °C in its TPR profile. As discussed in XRD section, the existence of independent oxides implies that the interaction between active components and ceria in the catalyst prepared by a co-precipitation method is extremely weak, which hinders the dispersion of CuO_x and MnO_x. Thus the only one reduction peak of CuMC-CP could be attributed to the reduction of the whole copper species and manganese species. For CuMC-IM, there are three reduction peaks in the H_2 consumption profile. The peak at about 185 °C is attributed to the reduction of highly dispersed copper and manganese species on the surface of CeO_2, and the other two peaks at about 250 °C are attributed to the reduction of a mixture of crystalline CuO and Cu^{+}

species. Compared to CuMC-CP, the presence of a small amount of Cu^+ species in CuMC-IM may account for its higher activity.

3.2.6. X-ray photoelectron spectroscopy (XPS)

Fig. 8 shows the XPS spectra of Cu $2p_{3/2}$, Mn $2p_{3/2}$ and Ce 3d for $CuO–MnO_x–CeO_2$ catalysts prepared by different methods. Binding energy is calibrated with C 1s = 284.8 eV. The corresponding composition of Cu and Mn species as well as the surface contents of Cu and Mn derived by XPS is listed in Table 2. As reported in previous literatures [3,17], for the Cu $2p_{3/2}$, the peak greater than 933.1 eV is one important XPS characteristic of Cu^{2+}/CuO while the peak at about 932.2–933.1 eV is the characteristic of Cu^+/Cu_2O. From Fig. 8, it is apparent that CuO_x species presenting in CuMC-HY is in a +1 oxidation state owing to the absence of a shake-up peak expected for Cu^{2+} at about 945.0 eV. Some Cu^+ species also presents in CuMC-IM, while CuO_x species in the other two catalysts are mainly in a +2 oxidation state with the $2p_{3/2}$ shifting to higher binding energies. However, the Cu $2p_{3/2}$ binding energies cannot be used to distinguish Cu_2O and CuO because they are essentially identical. According to literature [17], the Auger L_3VV electron lines of Cu are used to circumvent this problem, according to the peak of Cu^{2+} species around 917.1 eV and the one of Cu^+ species around 914.9 eV. The deconvolution results of Fig. 8 are listed in Table 2. The values of Cu^+/Cu^{2+} for CuMC-HY, CuMC-IM, CuMC-CP and CuMC-SG are 0.41, 0.21, 0.05 and 0.04, respectively. Moreover, the relative abundance of Cu^+ species on the surface is the highest in the case of CuMC-HY, which is beneficial to the selective oxidation of CO. In addition, the Cu contents on the surface for four samples are higher than the value of theoretical calculation (6.1 at.%), induced by the significant enrichment of copper oxide species on the ceria surface. CuMC-HY shows the lowest Cu content (only 19.0 at.%) among the four samples, indicating that the hydrothermal process facilitates the incorporation of more copper ions into the ceria lattice.

The deconvolution of the Mn $2p_{3/2}$ signal is useful to distinguish the states of Mn^{2+}, Mn^{3+} and Mn^{4+} with binding energy values of about 640.3, 641.3 and 642.7 eV, respectively. As shown in Table 2, the actual ratio of manganese to copper on the surface of CuMC-HY is 0.37, noticeably higher than the theoretical ratio 0.2, with Mn existing mainly as Mn^{4+} oxidation state, whereas those on the surface of CuMC-IM and CuMC-SG is 0.23 and 0.18, respectively, similar to the theoretical ratio, with the similar contents of Mn^{2+}, Mn^{3+} and Mn^{4+}. However, the actual ratio of manganese to copper on the surface of CuMC-CP is only 0.08, noticeably lower than the theoretical ratio, with Mn existing mainly as inactive Mn^{2+} oxidation state. The results indicate that the capability of the redox couple $Cu^{2+}–Cu^+$ in the catalyst CuMC-HY may be strongly enhanced by a large number of Mn^{4+} ions existing on the surface of CeO_2 [22], which is favorable for CO-PROX reaction in H_2-rich streams.

The oxidation states of Ce are analyzed by fitting the curves of Ce 3d spectra obtained from XPS measurements. As shown in Fig. 8, the binding energy of peaks of CuMC-CP is lower than that of the other three catalysts. According to the literature [44], the curves of Ce 3d spectra are composed of eight peaks corresponding to four pairs of spin–orbit doublets. Letters v and u refer to the $3d_{5/2}$ and $3d_{3/2}$ spin–obit components, respectively. The peaks labeled as v (ca. 882.4 eV), v″ (ca. 888.2 eV) and v‴ (ca. 898.3 eV) result from Ce^{4+} $3d_{5/2}$ while the peaks marked as u (ca. 900.8 eV), u″ (ca. 908.0 eV) and u‴ (ca. 916.4 eV) result from Ce^{4+} $3d_{3/2}$. The couples corresponding to one of the two possible electron configuration of the final state of the Ce^{3+} species are labeled as v′ (ca. 884.4 eV) and u′ (ca. 903.1 eV). The proportion of Ce^{3+} ions with regard to the total cerium is calculated from the ratio of the sum of areas of the Ce^{3+} species to the sum of areas of the total cerium species [44]. CuMC-CP exhibits higher relative concentration of Ce^{3+} $3d_{5/2}$ in Ce, compared with that of other catalysts, in good agreement with the results of XRD and HR-TEM analysis. The relative

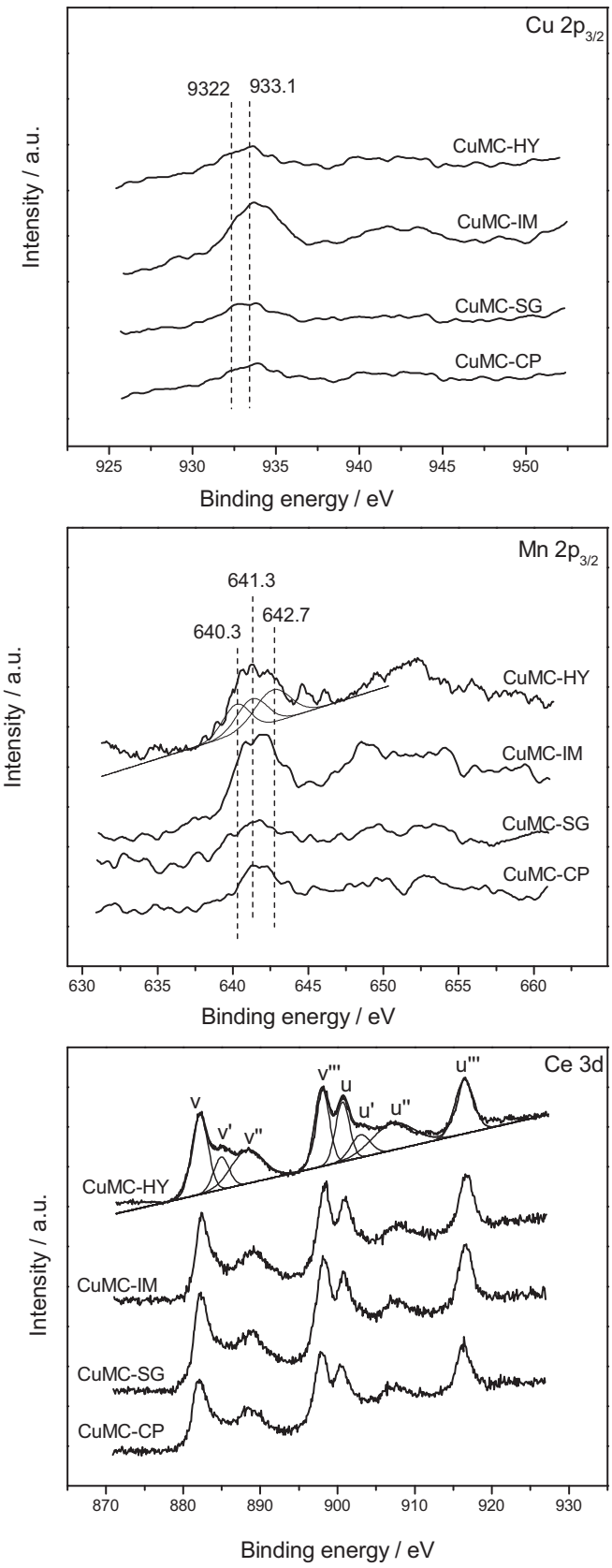

Fig. 8. XPS spectra of Cu $2p_{3/2}$, Mn $2p_{3/2}$ and Ce 3d for $CuO–MnO_x–CeO_2$ catalysts prepared by different methods.

concentration of Ce^{3+} $3d_{5/2}$ in Ce is obtained in Table 2 in the sequence of CuMC-CP > CuMC-HY > CuMC-SG > CuMC-IM, indicating that there are more oxygen vacancies presenting in the CeO_2 of CuMC-CP and CuMC-HY [44]. The interaction of CuO, MnO_x and CeO_2 species in CuMC-CP is very weak, so the formation of oxygen vacancies cannot improve the capability of the redox couple Cu^{2+}-Cu^{+}. However, for CuMC-HY, owing to the formation of stable Mn–Cu–Ce–O solid solution the formation of oxygen vacancies would enhance the formation of more Cu^{+} species, which may account for CuMC-HY's high activity for CO oxidation.

4. Conclusion

Four CuO–MnO_x–CeO_2 catalysts were prepared by hydrothermal, co-precipitation, impregnation, and citrate sol–gel methods, respectively. The results show that CuMC-HY exhibits the best catalytic performance for CO-PROX reaction in H_2-rich streams. T_{50} of CuMC-HY is only 74 °C, and the width of temperature window of CO conversions (up to 99.0%) is about 40 °C, from 110 to 140 °C. Moreover, CuMC-HY still removes CO to below 100 ppm at lower temperatures (140–150 °C) when 15% CO_2 and 7.5% H_2O are introduced into the reaction gas. The superior catalytic performance of CuMC-HY is mainly attributed to the stronger synergistic interaction between active components and ceria, the formation of Mn–Cu–Ce–O solid solution, the unique pore structure, and the existence of a large number of Cu^{+} species and Mn^{4+} species as well as oxygen vacancies. The sequence of catalytic activity of CuO–MnO_x–CeO_2 catalysts prepared by different methods for CO-PROX reaction is as follows: CuMC-HY > CuMC-SG > CuMC-IM > CuMC-CP. Despite the aggregation of copper species on the ceria surface, CuMC-IM still shows good catalytic activity due to the existence of a small amount of Mn–Cu–Ce–O solid solution as well as some Cu^{+} species in the catalyst. CuMC-CP exhibits the worst catalytic activity among the four CuO–MnO_x–CeO_2 catalysts, which is possibly related to the existence of independent CuO_x and MnO_x oxides leading to the weak interaction between active components and ceria in the catalyst.

Acknowledgements

We gratefully acknowledge the financial support from the Ministry of Science and Technology of China (No. 2011AA03A406) as well as Science and Technology Department of Zhejiang Province (No. 2009R50020).

References

[1] C.R. Jung, A. Kundu, S.W. Nam, H.-I. Lee, Appl. Catal. B: Environ. 84 (2008) 426–432.
[2] E.D. Park, D. Lee, H.C. Lee, Catal. Today 139 (2009) 280–290.
[3] Y.-Z. Chen, B.-J. Liaw, W.-C. Chang, C.-T. Huang, Int. J. Hydrogen Energy 32 (2007) 4550–4558.
[4] C.R. Jung, A. Kundu, S.W. Nam, H.-I. Lee, Appl. Catal. A: Gen. 331 (2007) 112–120.
[5] Q. Guo, Y. Liu, Appl. Catal. B: Environ. 82 (2008) 19–26.
[6] F.B. Derekaya, C. Kutar, Ç. Güldür, Mater. Chem. Phys. 115 (2009) 496–501.
[7] A. Martínez-Arias, D. Gamarra, M. Fernández-García, A. Hornés, P. Bera, Zs. Koppány, Z. Schay, Catal. Today 143 (2009) 211–217.
[8] S. Scirè, C. Crisafulli, S. Minicò, G.G. Condorelli, A.D. Mauro, J. Mol. Catal. A: Chem. 284 (2008) 24–32.
[9] M. Daté, M. Haruta, J. Catal. 201 (2001) 221–224.
[10] M.J. Kahlich, H.A. Gasteiger, R.J. Behm, J. Catal. 171 (1997) 93–105.
[11] D.H. Kim, M.S. Lim, Appl. Catal. A: Gen. 224 (2002) 27–38.
[12] G. Avgouropoulos, T. Ioannides, H.K. Matralis, J. Batista, S. Hocevar, Catal. Lett. 73 (2001) 33–40.
[13] C.R. Jung, J. Han, S.W. Nam, T.-H. Lim, S.-A. Hong, H.-I. Lee, Catal. Today 93–95 (2004) 183–190.
[14] Z. Liu, R. Zhou, X. Zheng, J. Mol. Catal. A: Chem. 267 (2007) 137–142.
[15] C.M. Bae, J.B. Ko, D.H. Kim, Catal. Commun. 6 (2005) 507–511.
[16] G. Avgouropoulos, T. Ioannides, Appl. Catal. B: Environ. 67 (2006) 1–11.
[17] Y.-Z. Chen, B.-J. Liaw, H.-C. Chen, Int. J. Hydrogen Energy 31 (2006) 427–435.
[18] D. Gamarra, A. Martínez-Arias, J. Catal. 263 (2009) 189–195.
[19] K. Sirichaiprasert, A. Luengnaruemitchai, S. Pongstabodee, Int. J. Hydrogen Energy 32 (2007) 915–926.
[20] Z. Wu, H. Zhu, Z. Qin, H. Wang, L. Huang, J. Wang, Appl. Catal. B: Environ. 98 (2010) 204–212.
[21] A.A. Firsova, A.N. Il'ichev, T.I. Khomenko, L.V. Gorobinskii, Yu.V. Maksimov, I.P. Suzdalev, V.N. Korchak, Kinet. Catal. 48 (2007) 282–291.
[22] J. Li, P. Zhu, S. Zuo, Q. Huang, R. Zhou, Appl. Catal. A: Gen. 381 (2010) 261–266.
[23] D.H. Kim, J.E. Cha, Catal. Lett. 86 (2003) 107–112.
[24] P. Zhu, J. Li, S. Zuo, R. Zhou, Appl. Surf. Sci. 255 (2008) 2903–2909.
[25] M.-F. Luo, Y.-P. Song, X.-Y. Wang, G.-Q. Xie, Z.-Y. Pu, P. Fang, Y.-L. Xie, Catal. Commun. 8 (2007) 834–838.
[26] F. Mariño, C. Descorme, D. Duprez, Appl. Catal. B: Environ. 58 (2005) 175–183.
[27] G. Avgouropoulos, T. Ioannides, H. Matralis, Appl. Catal. B: Environ. 56 (2005) 87–93.
[28] K.S.W. Sing, D.H. Everett, R.A.W. Haul, L. Moscou, R.A. Pierotti, J. Rouquérol, T. Siemieniewska, Pure Appl. Chem. 57 (1985) 603–619.
[29] Y. Zhang, H. Liang, X.Y. Gao, Y. Liu, Catal. Commun. 10 (2009) 1432–1436.
[30] X. Du, Z. Yuan, L. Cao, C. Zhang, S. Wang, Fuel Process. Technol. 89 (2008) 131–138.
[31] Y. She, Q. Zheng, L. Li, Y. Zhan, C. Chen, Y. Zheng, X. Lin, Int. J. Hydrogen Energy 34 (2009) 8929–8936.
[32] W. Shan, Z. Feng, Z. Li, J. Zhang, W. Shen, C. Li, J. Catal. 228 (2004) 206–217.
[33] Q. Liang, X. Wu, D. Weng, H. Xu, Catal. Today 139 (2008) 113–118.
[34] C. Gu, S. Lu, J. Miao, Y. Liu, Y. Wang, Int. J. Hydrogen Energy 35 (2010) 6113–6122.
[35] X. Wang, J.A. Rodriguez, J.C. Hanson, D. Gamarra, A. Martínez-Arias, M. Fernández-García, J. Phys. Chem. B 109 (2005) 19595–19603.
[36] D. Gamarra, G. Munuera, A.B. Hungría, M. Fernández-García, J.C. Conesa,.P.A. Midgley, X.Q. Wang, J.C. Hanson, J.A. Rodríguez, A. Martínez-Arias, J. Phys. Chem. C 111 (2007) 11026–11038.
[37] Z. Liu, Y. Chen, J. Catal. 177 (1998) 314–324.
[38] J. Papavasiliou, G. Avgouropoulos, T. Ioannides, J. Catal. 25 (2007) 7–20.
[39] M.R. Morales, B.P. Barbero, L.E. Cadús, Appl. Catal. B: Environ. 67 (2006) 229–236.
[40] S. Kato, R. Fujimaki, M. Ogasawara, T. Wakabayashi, Y. Nakahara, S. Nakata, Appl. Catal. B: Environ. 89 (2009) 183–188.
[41] Z. Liu, R. Zhou, X. Zheng, Int. J. Hydrogen Energy 33 (2008) 791–796.
[42] W.-P. Dow, T.-J. Huang, J. Catal. 160 (1996) 171–182.
[43] Z. Yang, B. He, Z. Lu, K. Hermansson, J. Phys. Chem. C 114 (2010) 4486–4494.
[44] J. Fan, X. Wu, X. Wu, Q. Liang, R. Ran, D. Weng, Appl. Catal. B 81 (2008) 38–48.